



Quantum nonreciprocity based on electromagnetically induced transparency in chiral quantum-optical systems

Yu You ^{1,2} Yiqi Hu ^{1,2} Gongwei Lin,^{1,*} Yihong Qi,^{1,†} Yueping Niu,^{1,3,‡} and Shangqing Gong^{1,3}

¹*Department of Physics, East China University of Science and Technology, Shanghai 200237, China*

²*School of Materials Science and Engineering, East China University of Science and Technology, Shanghai 200237, China*

³*Shanghai Engineering Research Center of Hierarchical Nanomaterials, Shanghai 200237, China*



(Received 23 December 2020; accepted 20 May 2021; published 10 June 2021)

On-chip single-photon nonreciprocal devices with high isolation and low insertion loss become a key element in quantum information processing. Based on electromagnetically induced transparency in chiral quantum systems, a single-photon isolator and a single-photon circulator are obtained without requiring unbalanced coupling. These devices have high isolation and low insertion loss. Moreover, their bandwidths are significantly broadened with the assistance of electromagnetically induced transparency.

DOI: [10.1103/PhysRevA.103.063706](https://doi.org/10.1103/PhysRevA.103.063706)

I. INTRODUCTION

Optical nonreciprocal devices, such as isolators and circulators which protect sources from being affected by the reflected light or direct light into the desired directions [1,2], play important roles in optical quantum communications and optical information processing. Early nonreciprocal photonic devices based on magneto-optical effects are unable to be miniaturized and integrated due to the bulky magnets [3,4]. Various schemes in nonmagnetic systems have been proposed to realize optical nonreciprocal components such as in nonlinear optical materials [5,6], parity-time optical coupled systems [7,8], asymmetric cavities [9], dynamic photonic structures [10–13], optomechanical systems [14–23], and cold or hot atomic ensembles [24–32].

As an exciting development, chiral quantum systems have shown unique advantages in the realization of on-chip single-photon nonreciprocal components, where the nonreciprocity depends on the spin of the emitter [33–37]. Moreover, due to the fact that the chiral quantum systems can be operated at the level of single emitters, these single-photon nonreciprocal components can be prepared in a coherent superposition of the operational states of the single emitters and thus are compatible with the photon-emitter entanglement, which plays an important role in quantum information processing [33]. In such systems, the single-photon isolators and circulators are theoretically proposed [34,35,38] and experimentally implemented [36,37]. However, these single-photon devices [34–38] require highly unbalanced coupling.

Electromagnetically induced transparency (EIT) is a laser-induced quantum interference effect that makes a resonant opaque medium highly transparent. The EIT effect has many

important applications in manipulating quantum information with single photons, for example, to achieve quantum reversible mapping [39–41], quantum logic gates [42,43], and quantum entangled states [44,45]. Here, we propose a scheme for single-photon optical nonreciprocity based on EIT in chiral quantum optical systems. Taking advantage of the EIT effect, a single-photon optical isolator and a single-photon optical circulator can be realized with high isolation and low insertion loss. Compared with the previous works in chiral quantum systems with highly unbalanced coupling [34–38], the proposed scheme here has two significant disadvantages: (i) optical nonreciprocity can be realized without unbalanced coupling; therefore, careful selection of special atomic energy levels with large transition difference is not necessary; and (ii) the bandwidths of the single-photon isolator and circulator are broadened by EIT.

II. THE MODEL SYSTEM

To begin with, we consider a single emitter coupled to chiral structures to realize optical nonreciprocity. The emitter has two degenerate transitions with different spin-polarized states σ_{\pm} and dipole moments μ_{\pm} . Due to the transversely strong confinement for guided light, the polarization of light is spin-momentum locking in the chiral systems; i.e., the light polarization depends on the propagation direction of light. Thus, we can assume that the right-propagating (left-propagating) light is perfectly right-hand circular (σ_{+} (left-hand circular σ_{-}) polarized, which only drives the σ_{+} (σ_{-}) spin-polarized transition of the emitter. As in the previous works on optical nonreciprocity in chiral systems [34–37], if $\mu_{+}/\mu_{-} \gg 1$, i.e., there is highly unbalanced coupling, optical nonreciprocity can be obtained at both sides near the resonant frequency. However, if μ_{+}/μ_{-} is not large enough, particularly when $\mu_{+}/\mu_{-} \sim 1$, the desired nonreciprocity disappears. Different from, though also inspired by, those works based on highly unbalanced coupling [34–37], we utilize a driving field to control one of the degenerate transitions

*gwlin@ecust.edu.cn

†qiyihong@ecust.edu.cn

‡niuyup@ecust.edu.cn

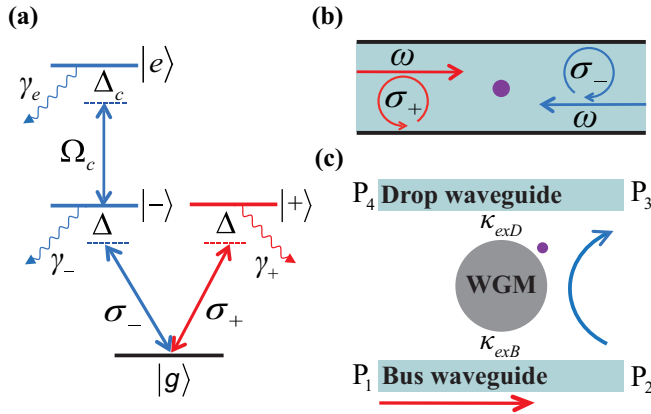


FIG. 1. (a) Energy level structure of the single emitter. (b) Schematic of the single-photon isolator. (c) Schematic of the single-photon circulator.

via EIT effect. In this way, high-performance single-photon nonreciprocity can be realized even without requiring unbalanced coupling.

In this paper, a single-photon isolator and a single-photon circulator can be realized with the single emitter coupled to a single-mode waveguide and a whispering gallery mode (WGM) resonator, respectively. The energy level structure of the single emitter is presented in Fig. 1(a). $|g\rangle$ denotes the ground state of the emitter with the energy ω_g . $|i\rangle$ ($i = +, -, e$) represents the excited state of the emitter with the energy ω_i and the decay rate γ_i , where $\omega_+ = \omega_-$. The transition from the ground state $|g\rangle$ to the degenerate state $|\pm\rangle$ with the dipole moment μ_{\pm} is only coupled to σ_{\pm} -polarized photons with the detuning $\Delta = \omega_{\pm} - \omega_g - \omega$, where ω represents the frequency of the incident photons. The coupling field with the frequency ω_c drives the transition between the state $|- \rangle$ and the state $|e\rangle$ with the semi-Rabi frequency $\Omega_c = \frac{\mu_{e-} \cdot \vec{E}_c}{2\hbar}$ and the detuning $\Delta_c = \omega_e - \omega_- - \omega_c$. Thus, the energy structure of the single emitter can be considered as two dependent parts: one is a simple two-level structure and the other is a ladder-type EIT three-level structure.

III. ISOLATOR

As in Fig. 1(b), a low-loss single-polarized single-mode (SPSM) waveguide is coupled to the single emitter so that a single-photon isolator can be realized. When a single photon is input from the left side of the waveguide, the polarization of light is right-hand circular (σ_+) and thus it only interacts with the transition between $|g\rangle$ and $|+\rangle$. In this case, the single emitter can be simplified into a two-level system and the Hamiltonian \hat{H}_+ of the system is given by

$$\begin{aligned} \hat{H}_+ = & \int dx \hat{C}_+^\dagger(x) \left(\omega_0 - iv_g \frac{\partial}{\partial x} \right) \hat{C}_+(x) \\ & + V_+ \int dx \delta(x) [\hat{C}_+(x) \hat{S}_{+g} + \hat{C}_+^\dagger(x) \hat{S}_{g+}] \\ & + (\omega_q - i\gamma_+) \hat{a}_+^\dagger \hat{a}_+. \end{aligned} \quad (1)$$

The corresponding eigenstate $|\psi_+(x, t)\rangle$ of the system for a single photon with the eigenvalue ω can be expanded as

$$\begin{aligned} |\psi_+(x, t)\rangle &= e^{-i\omega t} |\psi_+(x)\rangle \\ &= e^{-i\omega t} \left[\int dx \phi_+(x) \hat{C}_+^\dagger(x) + e_{+g} \hat{a}_+^\dagger \hat{a}_g \right] |0_c, g\rangle. \end{aligned} \quad (2)$$

When a single photon is incident from the right side of the waveguide, the light is left-propagating σ_- polarized and thus only couples to the transition between $|g\rangle$ and $|- \rangle$. If an external field Ω_c is applied to control the transition between $|- \rangle$ and $|e\rangle$, the EIT effect can take place. In this case, the single emitter can be considered as a three-level system and the Hamiltonian \hat{H}_- of the system is as follows [46]:

$$\begin{aligned} \hat{H}_- = & \int dx \hat{C}_-^\dagger(x) \left(\omega_0 + iv_g \frac{\partial}{\partial x} \right) \hat{C}_-(x) \\ & + V_- \int dx \delta(x) [\hat{C}_-(x) \hat{S}_{-g} + \hat{C}_-^\dagger(x) \hat{S}_{g-}] \\ & + (\omega_q + \Delta_c - i\gamma_e) \hat{a}_e^\dagger \hat{a}_e + (\omega_q - i\gamma_-) \hat{a}_-^\dagger \hat{a}_- \\ & + \Omega_c [\hat{a}_-^\dagger \hat{a}_e + \hat{a}_e^\dagger \hat{a}_-]. \end{aligned} \quad (3)$$

The corresponding eigenstate $|\psi_-(x, t)\rangle$ of the system for a single photon with the eigenvalue ω is

$$\begin{aligned} |\psi_-(x, t)\rangle &= e^{-i\omega t} |\psi_-(x)\rangle \\ &= e^{-i\omega t} \left[\int dx \phi_-(x) \hat{C}_-^\dagger(x) + e_{eg} \hat{a}_e^\dagger \hat{a}_g \right. \\ & \quad \left. + e_{-g} \hat{a}_-^\dagger \hat{a}_g \right] |0_c, g\rangle. \end{aligned} \quad (4)$$

In Eqs. (1)–(4), $\hat{C}_+(x)$ [$\hat{C}_-(x)$] represents a bosonic operator which can annihilate a right-propagating σ_+ -polarized (left-propagating σ_- -polarized) photon at the position x . \hat{a}_i ($i = g, +, -, e$) is the annihilation operator of the quantum state $|i\rangle$ and $\hat{S}_{ij} = \hat{a}_i^\dagger \hat{a}_j$ ($i, j = g, +, -, e$). The coupling strength V_{\pm} between the single emitter and the σ_{\pm} -polarized waveguide mode is proportional to the dipole moment μ_{\pm} . ω_0 are the intrinsic frequency of the waveguide and v_g is the group velocity of the single photon in the waveguide. Here, we define $\omega_{\pm} \equiv \omega_q$ and the ground-state energy of the single emitter is taken to be zero ($\omega_g \equiv 0$).

In Eqs. (2) and (4), $\phi_+(x)$ [$\phi_-(x)$] represents the single-photon wave function of the right-propagating (left-propagating) mode at the position x and e_{ig} ($i = +, -, e$) indicates the excitation amplitude of the single emitter in the state $|i\rangle$. $|0_c, g\rangle$ implies the original state of the system with zero photons in the waveguide and with the single emitter in the ground state $|g\rangle$. In order to solve the transmission amplitude of the incident single photon, we use $\phi_+(x) = e^{i(\omega - \omega_0)/v_g x} [\theta(-x) + t_+ \theta(x)]$ for the right-propagating σ_+ -polarized photon and $\phi_-(x) = e^{-i(\omega - \omega_0)/v_g x} [t_- \theta(-x) + \theta(x)]$ for the left-propagating σ_- -polarized photon at position x [47], where t_+ (t_-) is the transmission amplitude for the right-propagating σ_+ -polarized (left-propagating σ_- -polarized) single photon. $\theta(x)$ is the Heaviside step function in which $\theta(x)|_{x=0} = \frac{1}{2}$, $\frac{\partial \theta(x)}{\partial x}|_{x=0^+} = 1$, and $\frac{\partial \theta(-x)}{\partial x}|_{x=0^-} = -1$ [46,48].

According to the theory of single-photon transport in a single-mode waveguide in real-space [46,48], we can derive the steady-state transmission of the incident single photon with frequency ω in the configuration shown in Fig. 1(b). In the steady state, using the eigenequation of Hamiltonian $\hat{H}|\psi(x)\rangle = \hbar\omega|\psi(x)\rangle$ ($\hbar \equiv 1$), we can obtain

$$\omega_0\phi_+(0) - iv_g \left. \frac{\partial\phi_+(x)}{\partial x} \right|_{x=0} + V_+e_{+g}(0) = \omega\phi_+(0), \quad (5a)$$

$$V_+\phi_+(0) + (\omega_q - i\gamma_+)e_{+g}(0) = \omega e_{+g}(0), \quad (5b)$$

for a right-propagating single photon at the position $x = 0$. For a left-propagating single photon, we can obtain

$$\omega_0\phi_-(0) + iv_g \left. \frac{\partial\phi_-(0)}{\partial x} \right|_{x=0} + V_-e_{-g}(0) = \omega\phi_-(0), \quad (6a)$$

$$V_-\phi_-(0) + (\omega_q + \Delta_c - i\gamma_e)e_{eg}(0) + \Omega_c e_{-g}(0) = \omega e_{eg}(0), \quad (6b)$$

$$\Omega_c e_{eg}(0) + (\omega_q - i\gamma_-)e_{-g}(0) = \omega e_{-g}(0). \quad (6c)$$

Then we can further derive the transmission amplitudes of the right-propagating single photon and the left-propagating single photon given by

$$t_+(\omega) = \frac{\Delta - i(\gamma_+ - \Gamma_+)}{\Delta - i(\gamma_+ + \Gamma_+)}, \quad (7a)$$

$$t_-(\omega) = \frac{(\Delta + \Delta_c - i\gamma_e)(\Delta - i\gamma_- + i\Gamma_-) - \Omega_c^2}{(\Delta + \Delta_c - i\gamma_e)(\Delta - i\gamma_- - i\Gamma_-) - \Omega_c^2}, \quad (7b)$$

where $\Gamma_{\pm} = \frac{V_{\pm}^2}{2v_g}$. It can be seen in Eqs. (7a) and (7b) that t_+ is consistent with the transmission amplitude in a single-mode waveguide coupled to a two-level emitter case [48] and that t_- is equivalent to the transmission amplitude in a ladder-type three-level single emitter case [46]. Without loss of reality, we consider that $\gamma_{\pm}, \Gamma_{\pm}$ are proportional to μ_{\pm}^2 and thus have $\gamma_+/\gamma_- = \Gamma_+/\Gamma_- = \mu_+^2/\mu_-^2$ in the following. Then t_+ can be rewritten as

$$t_+(\omega) = \frac{\Delta - i[\mu_+^2/\mu_-^2(\gamma_- - \Gamma_-)]}{\Delta - i[\mu_+^2/\mu_-^2(\gamma_- + \Gamma_-)]}. \quad (7c)$$

From Eqs. (7b) and (7c), the difference between t_- and t_+ mainly depends on Ω_c and μ_+/μ_- . One can predict that if the driving field Ω_c is turned on, the emitter becomes transparent for the left-propagating single photon due to EIT and opaque for the right-propagating single photon near the resonant frequency. In this situation, the asymmetric transmission is naturally created and Ω_c performs a dominant role rather than μ_+/μ_- . When the driving field Ω_c is turned off, the difference between μ_+ and μ_- becomes essential for realizing the nonreciprocity.

Here, we define the transmission $T_{\pm} = |t_{\pm}|^2$. To study the influence of EIT and the unbalanced coupling on the nonreciprocity in detail, we representatively plot the transmissions of the single photon in both propagation directions with the driving field Ω_c turned on and off in the balanced coupling case and highly unbalanced coupling case. As shown in Figs. 2(a) and 2(c), we can see that assisted

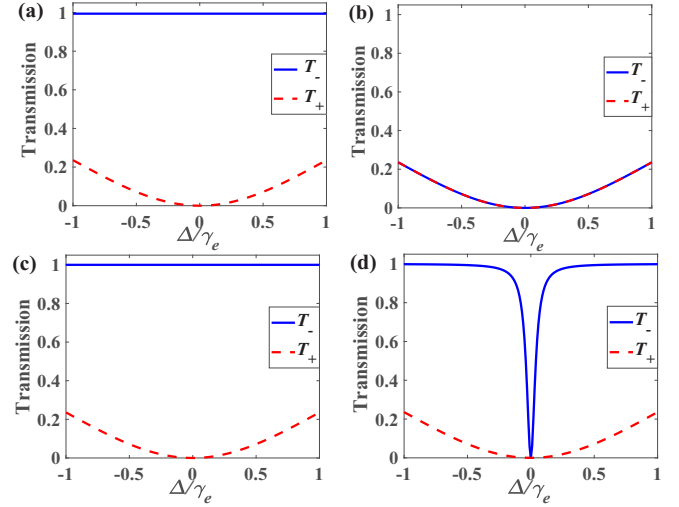


FIG. 2. Transmission of the single-photon isolator for (a) $\mu_+/\mu_- = 1$ and (c) $\mu_+/\mu_- = \sqrt{45}$ with EIT ($\Omega_c = 25\gamma_e$). Transmission of the single-photon isolator for (b) $\mu_+/\mu_- = 1$ and (d) $\mu_+/\mu_- = \sqrt{45}$ without EIT ($\Omega_c = 0$). Other parameters are $\gamma_+ = 0.9\gamma_e$, $\Gamma_{\pm} = \gamma_{\pm}$.

by EIT ($\Omega_c = 25\gamma_e$), when $\mu_+/\mu_- = 1$ (balanced coupling) and $\mu_+/\mu_- = \sqrt{45}$ (highly unbalanced coupling), the nonreciprocity always exists. Moreover, the left-propagating single photon can be mostly transmitted while the right-propagating single photon is totally absorbed in the transparency window. A high-performance single-photon isolator is realized with very high transmission and low insertion loss. However, if there is no EIT effect ($\Omega_c = 0$), only when μ_+/μ_- is large enough ($\mu_+/\mu_- = \sqrt{45}$) [35], the isolation function can be obtained, otherwise it will be greatly degraded and even disappear when $\mu_+/\mu_- = 1$ as shown in Figs. 2(b) and 2(d).

In order to intuitively show the performance of the single-photon isolator based on EIT and compare it with the isolators using highly unbalanced coupling [34–37], the contrast ratio $\eta \equiv \left| \frac{T_- - T_+}{T_- + T_+} \right|$ and the insertion loss $L \equiv -10\log_{10} T_-$ (dB) are plotted for $\mu_+/\mu_- = \sqrt{45}$ with EIT effect and without EIT effect in Figs. 3(a) and 3(b). It can be seen that the frequency regions of $\eta \geq 70\%$ and $L \leq 2$ dB are $0 \leq |\Delta|/\gamma_e \leq 0.84$ with EIT effect and $0.05 \leq |\Delta|/\gamma_e \leq 0.84$ without EIT effect. It is worth noting that with EIT the isolation bandwidth passes through the resonant frequency, while without EIT the

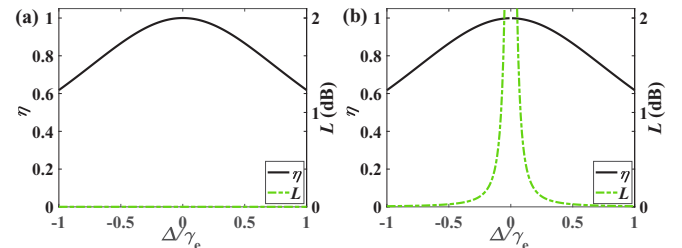


FIG. 3. Contrast ratio η and insertion loss L for $\mu_+/\mu_- = \sqrt{45}$ (a) with EIT ($\Omega_c = 25\gamma_e$) and (b) without EIT ($\Omega_c = 0$). Other parameters are the same as in Fig. 2.

isolation function disappears near the resonant region. Thus, it can be seen that the bandwidth of the single-photon isolator can be broadened by EIT.

IV. CIRCULATOR

To realize a single-photon circulator, a WGM microresonator is coupled to the single emitter with drop and bus waveguides guiding the single photon in and out as shown in Fig. 1(c). We assume that the counterclockwise mode of the WGM microresonator can be only excited by the σ_+ -polarized photon incident from P₁ or P₃ while the clockwise mode of the

WGM microresonator can be only excited by the σ_- -polarized photon incident from P₂ and P₄, in which P_{*i*} (*i* = 1, 2, 3, 4) denotes the port *i* of the circulator. Then we further assume that the σ_+ -polarized single photon can be scattered by the single emitter only into the counterclockwise mode or into an open environment. Due to the above assumptions, the single photon incident from P₁ can only exit from P₂ and P₄ while the single photon incident from P₂ can merely come out of P₁ and P₃.

When a single photon is input from port 1, the photon is σ_+ polarized and the Hamiltonian \hat{H}_+ of the system in this case can be obtained as follows:

$$\begin{aligned} \hat{H}_+ = & \int dx \hat{C}_{B_+}^\dagger(x) \left(\omega_0 - iv_g \frac{\partial}{\partial x} \right) \hat{C}_{B_+}(x) + \int dx V_B \delta(x) [\hat{C}_{B_+}^\dagger(x) \hat{a}_{c_+} + \hat{C}_{B_+}(x) \hat{a}_{c_+}^\dagger] + \int dx' \hat{C}_{D_+}^\dagger(x') \left(\omega_0 - iv_g \frac{\partial}{\partial x'} \right) \hat{C}_{D_+}(x') \\ & + \int dx' V_D \delta(x') [\hat{C}_{D_+}^\dagger(x') \hat{a}_{c_+} + \hat{C}_{D_+}(x') \hat{a}_{c_+}^\dagger] + \delta(x) (g_+ \hat{a}_{c_+}^\dagger \hat{S}_{g_+} + g_+^* \hat{a}_{c_+} \hat{S}_{+g}) + (\omega_c - i\kappa_i) \hat{a}_{c_+}^\dagger \hat{a}_{c_+} + (\omega_q - i\gamma_+) \hat{a}_{c_+}^\dagger \hat{a}_{c_+}. \end{aligned} \quad (8)$$

The corresponding eigenstate of the system $|\psi_+(x, t)\rangle$ for a single photon with the eigenvalue ω can be expanded as

$$|\psi_+(x, t)\rangle = e^{-i\omega t} |\psi_+(x)\rangle = e^{-i\omega t} \left[\int dx \phi_{B_+}(x) \hat{C}_{B_+}^\dagger(x) + \int dx' \phi_{D_+}(x') \hat{C}_{D_+}^\dagger(x') + e_{c_+} \hat{a}_{c_+}^\dagger + e_{eg} \hat{a}_{e_g}^\dagger \hat{a}_g \right] |0_p, 0_c, g\rangle. \quad (9)$$

When a single photon is incident from P₂, the Hamiltonian \hat{H}_- in this case can be expressed as

$$\begin{aligned} \hat{H}_- = & \int dx \hat{C}_{B_-}^\dagger(x) \left(\omega_0 + iv_g \frac{\partial}{\partial x} \right) \hat{C}_{B_-}(x) + \int dx V_B \delta(x) [\hat{C}_{B_-}^\dagger(x) \hat{a}_{c_-} + \hat{C}_{B_-}(x) \hat{a}_{c_-}^\dagger] + \int dx' \hat{C}_{D_-}^\dagger(x') \left(\omega_0 + iv_g \frac{\partial}{\partial x'} \right) \hat{C}_{D_-}(x') \\ & + \int dx' V_D \delta(x') [\hat{C}_{D_-}^\dagger(x') \hat{a}_{c_-} + \hat{C}_{D_-}(x') \hat{a}_{c_-}^\dagger] + \delta(x) (g_- \hat{a}_{c_-}^\dagger \hat{S}_{g_-} + g_-^* \hat{a}_{c_-} \hat{S}_{-g}) + \Omega_c (\hat{S}_{e_-} + \hat{S}_{-e}) + (\omega_q + \Delta_c - i\gamma_e) \hat{a}_e^\dagger \hat{a}_e \\ & + (\omega_q - i\gamma_-) \hat{a}_{c_-}^\dagger \hat{a}_{c_-} + (\omega_c - i\kappa_i) \hat{a}_{c_-}^\dagger \hat{a}_{c_-}. \end{aligned} \quad (10)$$

The corresponding eigenstate $|\psi_-(x, t)\rangle$ of the system for a single photon with the eigenvalue ω can be expanded as

$$\begin{aligned} |\psi_-(x, t)\rangle = & e^{-i\omega t} |\psi_-(x)\rangle \\ = & e^{-i\omega t} \left[\int dx \phi_{B_-}(x) \hat{C}_{B_-}^\dagger(x) \right. \\ & + \int dx' \phi_{D_-}(x') \hat{C}_{D_-}^\dagger(x') \\ & \left. + e_{c_-} \hat{a}_{c_-}^\dagger + e_{eg} \hat{a}_{e_g}^\dagger \hat{a}_g + e_{-g} \hat{a}_{-g}^\dagger \hat{a}_g \right] |0_p, 0_c, g\rangle. \end{aligned} \quad (11)$$

In Eqs. (8)–(11), $\hat{C}_{B_+}(x)$ [$\hat{C}_{B_-}(x)$] is a bosonic operator which can annihilate a right-propagating σ_+ -polarized (left-propagating σ_- -polarized) single photon in the bus waveguide at the position *x*. $\hat{C}_{D_+}(x')$ [$\hat{C}_{D_-}(x')$] is the annihilation operator for a right-propagating σ_+ -polarized (left-propagating σ_- -polarized) single photon in the drop waveguide at the position *x'*. The operator \hat{a}_{c_+} (\hat{a}_{c_-}) can annihilate the σ_+ -polarized counterclockwise (σ_- -polarized clockwise) resonator mode. V_B (V_D) is the coupling strength between the bus (drop) waveguide and the WGM microresonator. g_+ (g_-) is the coupling strength between the single emitter and the σ_+ -polarized counterclockwise (σ_- -polarized clockwise) resonator mode. γ_i (*i* = +, −, *e*) is the decay rate of the atomic state $|i\rangle$. We define the frequency of the degenerate transitions $\omega_\pm \equiv \omega_q \cdot \kappa_i$

is the intrinsic decay rate of the resonator. ω_c is the resonant frequency of the resonator.

In Eqs. (9) and (11), $\phi_{B_+}(x)$ [$\phi_{B_-}(x)$] presents the wave function of the single photon incident from port 1 (port 2) in the bus waveguide at the position *x*. $\phi_{D_+}(x')$ [$\phi_{D_-}(x')$] presents the wave function of the single photon incident from port 1 (port 2) in the drop waveguide at the position *x'*. $e_{c_i}(x)$ (*i* = +, −) is the excitation amplitude of the resonator. $|0_p, 0_c, g\rangle$ is the initial state of the system with no photon, no excitation of the resonator, and the single emitter. We have $\phi_{B_+}(x) = e^{i(\omega-\omega_0)/v_g x} [\theta(-x) + t_{12}\theta(x)]$ in the bus waveguide, $\phi_{D_+}(x') = t_{14} e^{-i(\omega-\omega_0)/v_g x'} \theta(-x')$ in the drop waveguide for the light incident from P₁, and $\phi_{B_-}(x) = e^{-i(\omega-\omega_0)/v_g x} [\theta(x) + t_{21}\theta(-x)]$ in the bus waveguide, $\phi_{D_-}(x') = t_{23} e^{i(\omega-\omega_0)/v_g x'} \theta(x')$ in the drop waveguide for the light incident from P₂ [47]. $\theta(x)$ is the Heaviside step function in which $\theta(x)|_{x=0} = \frac{1}{2}$, $\frac{\partial\theta(x)}{\partial x}|_{x=0_+} = 1$, and $\frac{\partial\theta(-x)}{\partial x}|_{x=0_-} = -1$ [46,48]. t_{ij} (*i, j* = 1, 2, 3, 4) is the transmission amplitude of the single photon incident from port *i* into port *j*.

In the steady state, using the eigenequation of Hamiltonian $\hat{H}|\psi(x)\rangle = \hbar\omega|\psi(x)\rangle$ ($\hbar \equiv 1$), we can obtain

$$t_{12}(\omega) = 1 + \frac{2i\kappa_{exB}}{\omega_c - \omega - i\kappa - \frac{|g_+|^2}{\omega_q - \omega - i\gamma_+}}, \quad (12a)$$

$$t_{14}(\omega) = \frac{2i\sqrt{\kappa_{exB}\kappa_{exD}}}{\omega_c - \omega - i\kappa - \frac{|g_+|^2}{\omega_q - \omega - i\gamma_+}}, \quad (12b)$$

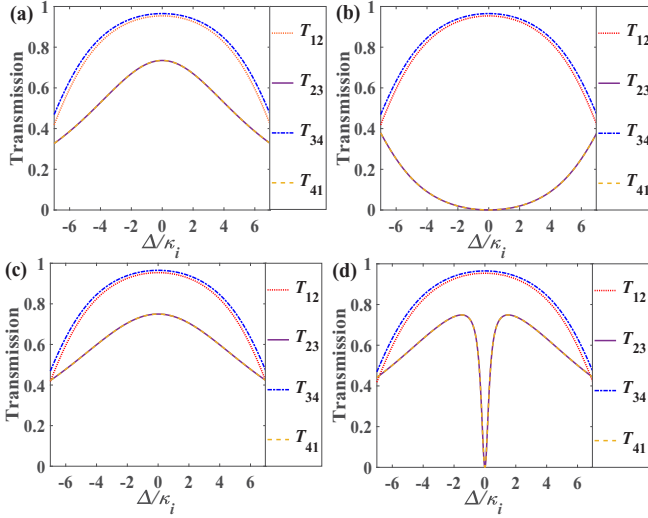


FIG. 4. Single-photon transmissions for (a) $\mu_+/\mu_- = 1$ and (c) $\mu_+/\mu_- = \sqrt{45}$ with EIT ($\Omega_c = 20\kappa_i$). Single-photon transmissions for (b) $\mu_+/\mu_- = 1$ and (d) $\mu_+/\mu_- = \sqrt{45}$ without EIT ($\Omega_c = 0$). Other parameters are $\kappa_{exB} = 4\kappa_i$, $\kappa_{exD} = 3\kappa_i$, $\Delta_c = 0$, $\gamma_+ = 0.3\kappa_i = 0.9\gamma_e$, and $g_+ = 10\kappa_i$.

for a single photon incident from P_1 , and

$$t_{21}(\omega) = 1 + \frac{2i\kappa_{exB}}{\omega_c - \omega - i\kappa - \frac{|g_-|^2}{\omega_q - \omega - i\gamma_- - \frac{\Omega_c^2}{\omega_q - \omega + \Delta_c - i\gamma_e}}}, \quad (13a)$$

$$t_{23}(\omega) = \frac{2i\sqrt{\kappa_{exB}\kappa_{exD}}}{\omega_c - \omega - i\kappa - \frac{|g_-|^2}{\omega_q - \omega - i\gamma_- - \frac{\Omega_c^2}{\omega_q - \omega + \Delta_c - i\gamma_e}}}, \quad (13b)$$

for a single photon input from P_2 , where $\Delta = \omega_c - \omega = \omega_q - \omega$ and $\kappa = \kappa_i + \kappa_{exB} + \kappa_{exD}$. κ_{exB} (κ_{exD}) represents the external decay rate of the microresonator to the bus (drop) waveguide. κ and κ_i are the total and intrinsic decay rates of the resonator, respectively. Here, we consider that γ_{\pm} , g_{\pm}^2 are proportional to μ_{\pm}^2 and thus we have the relations $\gamma_+/\gamma_- = g_+^2/g_-^2 = \mu_+^2/\mu_-^2$. Obviously, we can also obtain the transmission amplitudes t_{34} , t_{32} , t_{41} , and t_{43} by exchanging κ_{exB} and κ_{exD} in t_{12} , t_{14} , t_{23} , and t_{21} .

$T_{ij} = |t_{ij}|^2$ ($i, j = 1, 2, 3, 4$) is defined as the transmission for the single photon from port i to port j . We plot the transmission with EIT and without EIT in the balanced coupling case and highly unbalanced coupling case as in Sec. III. As shown in Figs. 4(a) and 4(c), the near-resonance transmissions are more than 75% in the direction of $P_1 \rightarrow P_2 \rightarrow P_3 \rightarrow P_4 \rightarrow P_1$. The four relatively high transmission windows can be simultaneously created no matter whether there is unbalanced coupling ($\mu_+/\mu_- = 1$ and $\mu_+/\mu_- = \sqrt{45}$). However, when the control field is turned off ($\Omega_c = 0$) and there is no EIT effect, T_{23} and T_{41} become very low and the single photon can only travel between P_1 (P_3) and P_2 (P_4) in the balanced coupling case ($\mu_+/\mu_- = 1$) as in Fig. 4(b). Without EIT, the highly unbalanced coupling (e.g., $\mu_+/\mu_- = \sqrt{45}$) becomes indispensable for realizing the circulator functionality shown in Fig. 4(d).

	1	2	3	4
1		0.95		0
2	0		0.75	
3		0		0.97
4	0.75		0.06	

Transmission matrix

FIG. 5. Transmission matrix of the single-photon circulator at the resonant frequency $\Delta = 0$. The row corresponds to the input port i and the column to the output port j . The values inside the color squares are the transmission between the two ports. Other parameters are the same as in Fig. 4.

From Fig. 5, assisted by EIT, a four-port single-photon circulator can be realized with high transmission and low insertion loss even without unbalanced coupling. The circulator can direct the resonant single photon incident from the input ports P_1 , P_2 , P_3 , and P_4 into the output ports P_2 , P_3 , P_4 , and P_1 with the transmissions $T_{12} = 95\%$, $T_{23} = 75\%$, $T_{34} = 97\%$, and $T_{41} = 75\%$, respectively, and block the single photon in the reverse direction.

We also plot the contrast ratio $\eta_{i,j} \equiv |T_{i,j} - T_{j,i}|$ and the insertion loss $L_{i,j} \equiv -10\log_{10} T_{i,j}$ (dB) ($\{i, j\} = \{1, 2\}, \{2, 3\}, \{3, 4\}, \{4, 1\}$) for $\mu_+/\mu_- = \sqrt{45}$ with EIT effect and without EIT effect in Fig. 6. We can find that the frequency regions of $\eta_{12}, \eta_{23}, \eta_{34}, \eta_{41} \geq 70\%$ and $L_{12}, L_{23}, L_{34}, L_{41} \leq 2$ dB are $0 \leq |\Delta|/\kappa_i \leq 2.73$ with EIT effect and $0.64 \leq |\Delta|/\kappa_i \leq 3.34$ without EIT effect. The

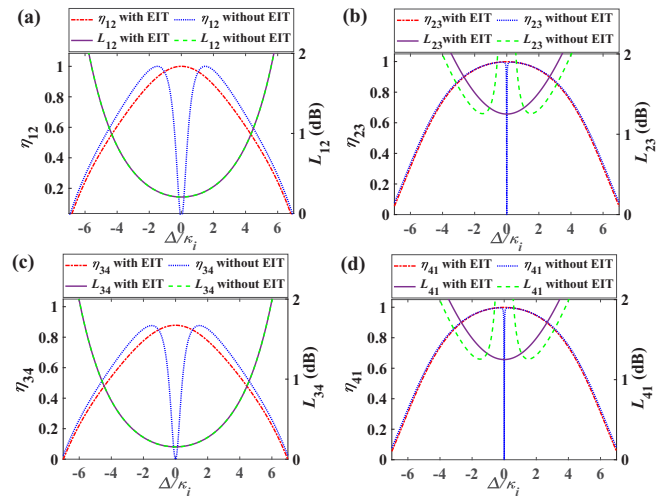


FIG. 6. Contrast ratio $\eta_{i,j}$ and insertion loss $L_{i,j}$ of the single-photon circulator for $\mu_+/\mu_- = \sqrt{45}$ with EIT ($\Omega_c = 20\kappa_i$) and without EIT ($\Omega_c = 0$) for (a) $\{i, j\} = \{1, 2\}$, (b) $\{i, j\} = \{2, 3\}$, (c) $\{i, j\} = \{3, 4\}$, and (d) $\{i, j\} = \{4, 1\}$. Other parameters are the same as in Fig. 4.

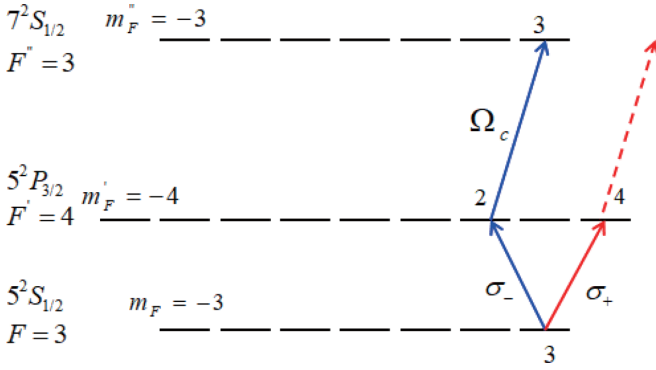


FIG. 7. The coupling scheme for experimental implementation.

optical nonreciprocity can be achieved near the resonant point and thus the bandwidth of the circulator is significantly broadened by EIT.

V. EXPERIMENTAL FEASIBILITY

Then we briefly discuss the experimental feasibility of the proposed scheme. According to the experiments on the single-photon isolator and circulator in chiral quantum optical systems [36,37], we can select the rubidium-85 atom as the single emitter and the hyperfine Zeeman state $|5^2S_{1/2}, F = 3, m_F = 3\rangle$ as the ground state. We then choose the Zeeman states $|5^2P_{3/2}, F' = 3, m_F' = 2\rangle$ and $|5^2P_{3/2}, F' = 3, m_F' = 4\rangle$ as the degenerate lower excited states. In order to construct an EIT structure, we further choose the Zeeman state $|7^2S_{1/2}, F'' = 3, m_F'' = 3\rangle$ as the highest excited state and exploit a control field Ω_c driving between the states $|5^2P_{3/2}, F' = 4, m_F' = 2\rangle$ and $|7^2S_{1/2}, F'' = 3, m_F'' = 3\rangle$ as shown in Fig. 7 [49]. As for the single-photon isolator, we consider the configuration of a single resonator-enhanced emitter coupled to a waveguide as in [36]. Thus, we can take $\Gamma_{\pm} = 2\pi \times 5$ MHz, $\gamma_+ = 2\pi \times 101.3$ MHz, $\gamma_- = 2\pi \times 7.8$ MHz [36], and consider $\gamma_e = 2\pi \times 0.724$ MHz and $\Omega_c = 2\pi \times 14$ MHz, and then the isolation contrast ratio η of 0.89% and the insertion loss L of 0.86 dB can be obtained at resonant frequency. For the single-photon circulator configuration, the WGM resonator which sustains two degenerate clockwise and counterclockwise modes coupled to one or two

waveguides has been demonstrated experimentally [36,37,50–52]. Within the existing technology, the clockwise (counterclockwise) mode of the resonator can overlap more than 96% with a circularly σ_+ -polarized (σ_- -polarized) mode due to the strong confinement for guided light [51]. By setting properly the polarization of light in the waveguides, the light can be almost completely coupled into the WGM resonator. With the choice of $g_+ = 2\pi \times 12$ MHz, $g_- = 2\pi \times 12/\sqrt{28}$ MHz, $\kappa_i = 2\pi \times 5$ MHz, $\kappa = \kappa_i + \kappa_{exB} + \kappa_{exD} = 2\pi \times 22$ MHz, $\kappa_{exB} = 2\pi \times 11$ MHz, $\gamma_{\pm} = 2\pi \times 3$ MHz [37], and taking $\gamma_e = 2\pi \times 0.724$ MHz, $\Omega_c = 2\pi \times 14$, we have the contrast ratio $\eta_{12} = 1$, $\eta_{23} = 0.82$, $\eta_{34} = 0.54$, and $\eta_{41} = 0.82$ and the insertion loss $L_{12} = 3.27$ dB, $L_{23} = 2.64$ dB, $L_{34} = 1.63$ dB, and $L_{41} = 2.64$ dB for resonant single photons. Furthermore, we can also reverse the optical nonreciprocity by initially preparing the ^{85}Rb atom into the state $|5^2S_{1/2}, F = 3, m_F = -3\rangle$.

VI. CONCLUSION

We propose a scheme for realizing single-photon nonreciprocity based on EIT in chiral structures coupled to a single emitter. Combining EIT with the unique coupling features in chiral quantum systems, a single-photon isolator and a single-photon circulator with high isolation and low insertion loss are obtained. With the help of EIT, the optical nonreciprocity can be realized near the resonant frequency and thus the bandwidth of the nonreciprocal window is significantly broadened. Moreover, the nonreciprocity does not require unbalanced quantum coupling. Thus, there is no need to select emitters with different transition strengths. We also propose a feasible coupling scheme, under which we evaluate the performance of two nonreciprocal devices using the experimental parameters. Our study may offer a promising approach to realizing single-photon nonreciprocity for scalable integrated optical circuits.

ACKNOWLEDGMENTS

This work was supported by the National Natural Science Foundation of China (Grants No. 11674094, No. 11774089, No. 11874146, No. 11981260012, and No. 12034007) and the Shanghai Natural Science Foundation (Grants No. 18ZR1410500 and No. 18DZ2252400).

Y.Y. and Y.H. contributed equally to this work.

- [1] D. Jalas, A. Petrov, M. Eich, W. Freude, S. H. Fan, Z. F. Yu, R. Baets, M. Popović, A. Melloni, J. D. Joannopoulos, M. Vanwolleghem, C. R. Doerr and H. Renner, What is—and what is not—an optical isolator, *Nat. Photonics* **7**, 579 (2013).
- [2] T. R. Zaman, X. Y. Guo, and R. J. Ram, Semiconductor waveguide isolators, *J. Lightwave Technol.* **26**, 0733 (2008).
- [3] M. C. Tien, T. Mizumoto, P. Pintus, H. Kromer, and J. E. Bowers, Silicon ring isolators with bonded nonreciprocal magneto-optic garnets, *Opt. Express* **19**, 11740 (2011).
- [4] L. Bi, J. J. Hu, P. Jiang, D. H. Kim, G. F. Dionne, L. C. Kimerling, and C. A. Ross, On-chip optical isolation in monolithically integrated non-reciprocal optical resonators, *Nat. Photonics* **5**, 758 (2011).
- [5] L. Fan, J. Wang, L. T. Varghese, H. Shen, B. Niu, Y. Xuan, A. M. Weiner, and M. H. Qi, An all-silicon passive optical diode, *Science* **335**, 447 (2012).
- [6] Y. Sun, Y. W. Tong, C. H. Xue, Y. Q. Ding, Y. H. Li, H. T. Jiang, and H. Chen, Electromagnetic diode based on nonlinear electromagnetically induced transparency in metamaterials, *Appl. Phys. Lett.* **103**, 091904 (2013).
- [7] L. Chang, X. S. Jiang, S. Y. Hua, C. Yang, J. M. Wen, L. Jiang, G. Y. Li, G. Z. Wang, and M. Xiao, Parity-time symmetry and variable optical isolation in active-passive-coupled microresonators, *Nat. Photonics* **8**, 524 (2014).
- [8] B. Peng, S. H. Kaya Özdemir, F. C. Lei, F. Monifi, M. Gianfreda, G. L. Long, S. H. Fan, F. Nori, C. M. Bender, and L. Yang, Parity-time-symmetric whispering-gallery microcavities, *Nat. Phys.* **10**, 394 (2014).

- [9] P. F. Yang, X. W. Xia, H. He, S. K. Li, X. Han, P. Zhang, G. Li, P. F. Zhang, J. P. Xu, Y. P. Yang, and T. C. Zhang, Realization of Nonlinear Optical Nonreciprocity on a Few-Photon Level Based on Atoms Strongly Coupled to an Asymmetric Cavity, *Phys. Rev. Lett.* **123**, 233604 (2019).
- [10] Z. F. Yu and S. H. Fan, Complete optical isolation created by indirect interband photonic transitions, *Nat. Photonics* **3**, 91 (2009).
- [11] M. S. Kang, A. Butsch, and P. St. J. Russell, Reconfigurable light-driven opto-acoustic isolators in photonic crystal fibre, *Nat. Photonics* **5**, 549 (2011).
- [12] K. J. Fang, Z. F. Yu, and S. H. Fan, Photonic Aharonov-Bohm Effect Based on Dynamic Modulation, *Phys. Rev. Lett.* **108**, 153901 (2012).
- [13] L. Q. Yuan, S. S. Xu, and S. H. Fan, Achieving nonreciprocal unidirectional single-photon quantum transport using the photonic Aharonov-Bohm effect, *Opt. Lett.* **40**, 5140 (2015).
- [14] M. Hafezi and P. Rabl, Optomechanically induced non-reciprocity in microring resonators, *Opt. Express* **20**, 7672 (2012).
- [15] X. W. Xu and Y. Li, Optical nonreciprocity and optomechanical circulator in three-mode optomechanical systems, *Phys. Rev. A* **91**, 053854 (2015).
- [16] Z. Shen, Y. L. Zhang, Y. Chen, C. L. Zou, Y. F. Xiao, X. B. Zou, F. W. Sun, G. C. Guo, and C. H. Dong, Experimental realization of optomechanically induced non-reciprocity, *Nat. Photonics* **10**, 657 (2016).
- [17] M. A. Miri, F. Ruesink, E. Verhagen, and A. Alù, Optical Nonreciprocity Based on Optomechanical Coupling, *Phys. Rev. Appl.* **7**, 064014 (2017).
- [18] N. R. Bernier, L. D. Tóth, A. Koottandavida, M. A. Ioannou, D. Malz, A. Nunnenkamp, A. K. Feofanov, and T. J. Kippenberg, Nonreciprocal reconfigurable microwave optomechanical circuit, *Nat. Commun.* **8**, 604 (2017).
- [19] Z. Shen, Y. L. Zhang, Y. Chen, F. W. Sun, X. B. Zou, G. C. Guo, C. L. Zou, and C. H. Dong, Reconfigurable optomechanical circulator and directional amplifier, *Nat. Commun.* **9**, 1797 (2018).
- [20] X. W. Xu, L. N. Song, Q. Zheng, Z. H. Wang, and Y. Li, Optomechanically induced nonreciprocity in a three-mode optomechanical system, *Phys. Rev. A* **98**, 063845 (2018).
- [21] G. L. Li, X. Xiao, and Y. Li, Tunable optical nonreciprocity and a phonon-photon router in an optomechanical system with coupled mechanical and optical modes, *Phys. Rev. A* **97**, 023801 (2018).
- [22] R. Freek, J. P. Mathew, and M. A. Miri, Optical circulation in a multimode optomechanical resonator, *Nat. Commun.* **9**, 1798 (2018).
- [23] B. J. Li, R. Huang, and X. W. Xu, Nonreciprocal unconventional photon blockade in a spinning optomechanical system, *Photonics Res.* **7**, 630 (2019).
- [24] M. X. Dong, Y. C. Yu, Y. H. Ye, W. H. Zhang, E. Li, L. Zeng, G. C. Guo, D. S. Ding, and B. S. Shi, Experimental realization of quantum non-reciprocity based on cold atomic ensembles, [arXiv:1908.09242](https://arxiv.org/abs/1908.09242).
- [25] P. F. Yang, M. Li, X. Han, H. He, and G. Li, Non-reciprocal cavity polariton, [arXiv:1911.10300](https://arxiv.org/abs/1911.10300).
- [26] S. C. Zhang, Y. Q. Hu, G. W. Lin, Y. P. Niu, K. Y. Xia, J. B. Gong, and S. Q. Gong, Thermal-motion-induced non-reciprocal quantum optical system, *Nat. Photonics* **12**, 744 (2018).
- [27] K. Y. Xia, F. Nori, and M. Xiao, Cavity-Free Optical Isolators and Circulators Using a Chiral Cross-Kerr Nonlinearity, *Phys. Rev. Lett.* **121**, 203602 (2018).
- [28] G. W. Lin, S. C. Zhang, and Y. Q. Hu, Nonreciprocal Amplification with Four-Level Hot Atoms, *Phys. Rev. Lett.* **123**, 033902 (2019).
- [29] Y. Q. Hu, S. C. Zhang, and Y. H. Qi, Multiwavelength Magnetic-Free Optical Isolator by Optical Pumping in Warm Atoms, *Phys. Rev. Appl.* **12**, 054004 (2019).
- [30] S. C. Zhang, G. W. Lin, and Y. Q. Hu, Cavity-Free Circulator with Low Insertion Loss Using Hot Atoms, *Phys. Rev. Appl.* **14**, 024032 (2020).
- [31] C. Liang, B. Liu, A. N. Xu, X. Wen, C. C. Lu, K. Y. Xia, M. K. Tey, Y. C. Liu, and L. You, Collision-Induced Broadband Optical Nonreciprocity, *Phys. Rev. Lett.* **125**, 123901 (2020).
- [32] N. Y. Jia, N. Schine, A. Georgakopoulos, A. Ryou, A. Sommer, and J. Simon, Photons and polaritons in a broken-time-reversal nonplanar resonator, *Phys. Rev. A* **97**, 013802 (2018).
- [33] P. Lodahl, S. Mahmoodian, S. Stobbe, A. Rauschenbeutel, P. Schneeweiss, and J. Volz, Chiral quantum optics, *Nature (London)* **541**, 473 (2017).
- [34] W. B. Yan, W. Y. Ni, J. Zhang, F. Y. Zhang, and H. Fan, Tunable single-photon diode by chiral quantum physics, *Phys. Rev. A* **98**, 043852 (2018).
- [35] K. Y. Xia, G. W. Lu, G. W. Lin, Y. Q. Cheng, Y. P. Niu, S. Q. Gong, and J. Twamley, Reversible nonmagnetic single-photon isolation using unbalanced quantum coupling, *Phys. Rev. A* **90**, 043802 (2014).
- [36] C. Sayrin, C. Junge, R. Mitsch, B. Albrecht, D. O'Shea, P. Schneeweiss, J. Volz, and A. Rauschenbeutel, Nanophotonic Optical Isolator Controlled by the Internal State of Cold Atoms, *Phys. Rev. X* **5**, 041036 (2015).
- [37] M. Scheucher, A. Hilico, E. Will, J. Volz, and A. Rauschenbeutel, Quantum optical circulator controlled by a single chirally coupled atom, *Science* **354**, 1577 (2016).
- [38] L. Tang, J. S. Tang, W. D. Zhang, G. W. Lu, H. Zhang, Y. Zhang, K. Y. Xia, and M. Xiao, On-chip chiral single-photon interface: Isolation and unidirectional emission, *Phys. Rev. A* **99**, 043833 (2019).
- [39] C. H. van der Wal, M. D. Eisaman, A. Andre, R. L. Walsworth, D. F. Phillips, A. S. Zibrov, and M. D. Lukin, Atomic Memory for Correlated Photon States, *Science* **301**, 196 (2003).
- [40] J. Appel, E. Figueroa, D. Korystov, M. Lobino, and A. I. Lvovsky, Quantum Memory for Squeezed Light, *Phys. Rev. Lett.* **100**, 093602 (2008).
- [41] K. S. Choi, H. Deng, J. Laurat, and H. J. Kimble, Mapping photonic entanglement into and out of a quantum memory, *Nature (London)* **452**, 67 (2008).
- [42] C. Ottaviani, D. Vitali, M. Artoni, F. Cataliotti, and P. Tombesi, Polarization Qubit Phase Gate in Driven Atomic Media, *Phys. Rev. Lett.* **90**, 197902 (2003).
- [43] D. Petrosyan, Towards deterministic optical quantum computation with coherently driven atomic ensembles, *J. Opt. B* **7**, S141 (2005).
- [44] M. Paternostro, and M. S. Kim, B. S. Ham, Generation of entangled coherent states via cross-phase-modulation in a double electromagnetically induced transparency regime, *Phys. Rev. A* **67**, 023811 (2003).
- [45] M. G. Payne and L. Deng, Quantum Entanglement of Fock States with Perfectly Efficient Ultraslow Single-Probe

- Photon Four-Wave Mixing, *Phys. Rev. Lett.* **91**, 123602 (2003).
- [46] D. Witthaut and A. S. Sørensen, Photon scattering by a three-level emitter in a one-dimensional waveguide, *New J. Phys.* **12**, 043052 (2010).
- [47] J.-T. Shen and S. Fan, Coherent photon transport from spontaneous emission in one-dimensional waveguides, *Opt. Lett.* **30**, 2001 (2005).
- [48] J.-T. Shen and S. Fan, Theory of single-photon transport in a single-mode waveguide. II. Coupling to a whispering-gallery resonator containing a two-level atom, *Phys. Rev. A* **79**, 023838 (2009).
- [49] S. Wielandy and A. L. Gaeta, Coherent Control of the Polarization of an Optical Field, *Phys. Rev. Lett.* **81**, 3359 (1998).
- [50] I. Shomroni, S. Rosenblum, Y. Lovsky, O. Bechler, G. Guendelman and B. Dayan, All-optical routing of single photons by a one-atom switch controlled by a single photon, *Science* **345**, 903 (2014).
- [51] C. Junge, D. O'Shea, J. Volz and A. Rauschenbeutel, Strong Coupling between Single Atoms and Nontransversal Photons, *Phys. Rev. Lett.* **110**, 213604 (2013).
- [52] D. O'Shea, C. Junge, J. Volz, and A. Rauschenbeutel, Fiber-Optical Switch Controlled by a Single Atom, *Phys. Rev. Lett.* **111**, 193601 (2013).